frontiers | Frontiers in Environmental Science

TYPE Original Research
PUBLISHED 18 April 2023
DOI 10.3389/fenvs.2023.1112143

OPEN ACCESS

EDITED BY
Yong Xiao,
Southwest Jiaotong University, China

REVIEWED BY
Polina Lemenkova,
Université libre de Bruxelles, Belgium
Bing Bai,
Beijing Jiaotong University, China

*CORRESPONDENCE
Kai Liu,
acaner@163.com
Yaoyao Zhang,
zhangyy@cags.ac.cn

SPECIALTY SECTION
This article was submitted to Freshwater Science, a section of the journal Frontiers in Environmental Science

RECEIVED 30 November 2022
ACCEPTED 29 March 2023
PUBLISHED 18 April 2023

CITATION
Liu K, Zhang Y, He Q, Zhang S, Jia W, He X, Zhang H, Wang L and Wang S (2023), Characteristics of thermophysical parameters in the Wugongshan area of South China and their insights for geothermal genesis.
Front. Environ. Sci. 11:1112143.
doi: 10.3389/fenvs.2023.1112143

Characteristics of thermophysical parameters in the Wugongshan area of South China and their insights for geothermal genesis

Kai Liu[1,2]*, Yaoyao Zhang[2]*, Qingcheng He[2], Shouchuan Zhang[2], Wuhui Jia[2], Xiaolong He[3], Haoran Zhang[4], Luyao Wang[2] and Shuxun Wang[5]

[1]School of Water Resources and Environment, China University of Geosciences (Beijing), Beijing, China, [2]Chinese Academy of Geological Sciences, Beijing, China, [3]School of Environment and Resources, Xiangtan University, Xiangtan, China, [4]College of Geoscience and Surveying Engineering, China University of Mining and Technology (Beijing), Beijing, China, [5]School of Earth Sciences and Resources, China University of Geosciences (Beijing), Beijing, China

The Wugongshan area is rich in medium–low temperature convective geothermal resources, among which there are more than 10 geothermal fields in Wentang, Wanlongshan, Wenjia, Hongjiang, etc. There are few basic geothermal geological studies in the geothermal fields and their peripheral areas; thus far, no systematic research work into the thermophysical parameters has been carried out. In this paper, 85 rock samples were collected from the surface and boreholes covering the strata and magmatic rocks in the study area. The results show that the average radioheat generation rate, the average thermal conductivity, and the average specific heat are 0.24–5.49 (μW/m^3), 1.995–4.390 (W/mK), and 1.318–4.829 (MJ/m^{3}K), respectively. The average thermal diffusivity ranges from 1.115 to 1.611 × 10^{-6} m^2/s. The highest radioheat generation rate is Jurassic granite, and the lowest is quartz vein. The largest thermal conductivity and specific heat is the siliceous quartzite, and the smallest is the quartz vein. The highest thermal diffusivity is Cambrian metamorphic mica schist, and the lowest is siliceous quartzite. The radioactive heat generation rate, thermal conductivity, specific heat, and thermal diffusivity are closely related to the chemical composition, mineral composition, rock fabric, porosity, water content, and temperature and pressure conditions of rocks in the whole area. There is a linear relationship between thermal conductivity (K) and thermal diffusivity (κ), and the correlation equation is K = −0.3144k + 3.2172. Combined with the characteristics of thermophysical parameters, the genetic theory of deep crust heat generation + structural heat accumulation + siliceous quartzite heat conduction + granite heat preservation is preliminarily proposed.

KEYWORDS

radioactive heat generation rate, thermal conductivity, heat source mechanism, geothermal genesis, Wugongshan area

1 Introduction

In recent years, with the shortage of fossil energy and the increasing environmental problems, renewable resources have become an important research topic. Geothermal energy is a renewable resource hidden in the earth. As one important solution to the energy crisis, it has attracted worldwide attention due to its advantages such as large resource potential, low development cost, and high utilization coefficient (Wang et al., 2015). The distribution of geothermal resources has obvious zonation and zonality in China (Wang and Lin, 2020). The Wugongshan medium–low temperature geothermal resources in Jiangxi Province are located in the south of the convergence belt of the Yangtze Block and the Cathaysia Block, which is composed of 15 geothermal fields with huge resource potential, such as Wentang geothermal field and Wanlongshan geothermal field (Xia et al., 2017; Gao et al., 2020).

The genetic mechanism of geothermal resources can be attributed to two separated processes, forming heat and transporting heat. The formation of crustal temperature is controlled by the radiogenic heat producing elements. The thermophysical parameters of rocks are the basic information for the thermal field and include thermal conductivity, specific heat capacity, thermal diffusivity, and radioactive heat generation rate. The thermophysical parameters of rocks directly affect the generation, storage, and transfer of heat between various layers in the earth interior, which are important for designing high-level waste repositories in the nuclear industry, developing ground source heat pumps (Liu et al., 2006; Wan et al., 2013; Wang et al., 2020; Zhou et al., 2017), and studying lithospheric thermal structures and basin thermal histories (Vila et al., 2010; Feng et al., 2018; Sven, 2018; Zhang et al., 2019). Most previous studies focus on the analysis of thermophysical parameters in sedimentary rocks (Cho et al., 2010). Few studies have reported the characteristics of the thermophysical parameters of granite rocks. The Wugongshan area is occupied by Jurassic granite, which provides convenient conditions for studying the thermophysical parameters in granite.

The heat transport process in porous media is controlled by the thermophysical parameters. Previous studies have revealed the relationships between the thermophysical parameters and basic physical properties (i.e., density, mineral composition, and water content). Côté and Konrad (2005) developed a model to introduce an empirical relationship between the normalized thermal conductivity and the degree of saturation. Lu et al. (2007) developed an improved model to rebuild the relationship between the thermal conductivity and the basic physical properties of unsaturated soils. Cho and Kwon, 2010 proposed empirical correlations to predict the thermal conductivity and the specific heat capacity of granite as a function of porosity and water content. However, there is still a lack of quantitative analysis of the non-linear relationship between thermophysical parameters and geothermal genesis mechanisms. The thermophysical analysis is a

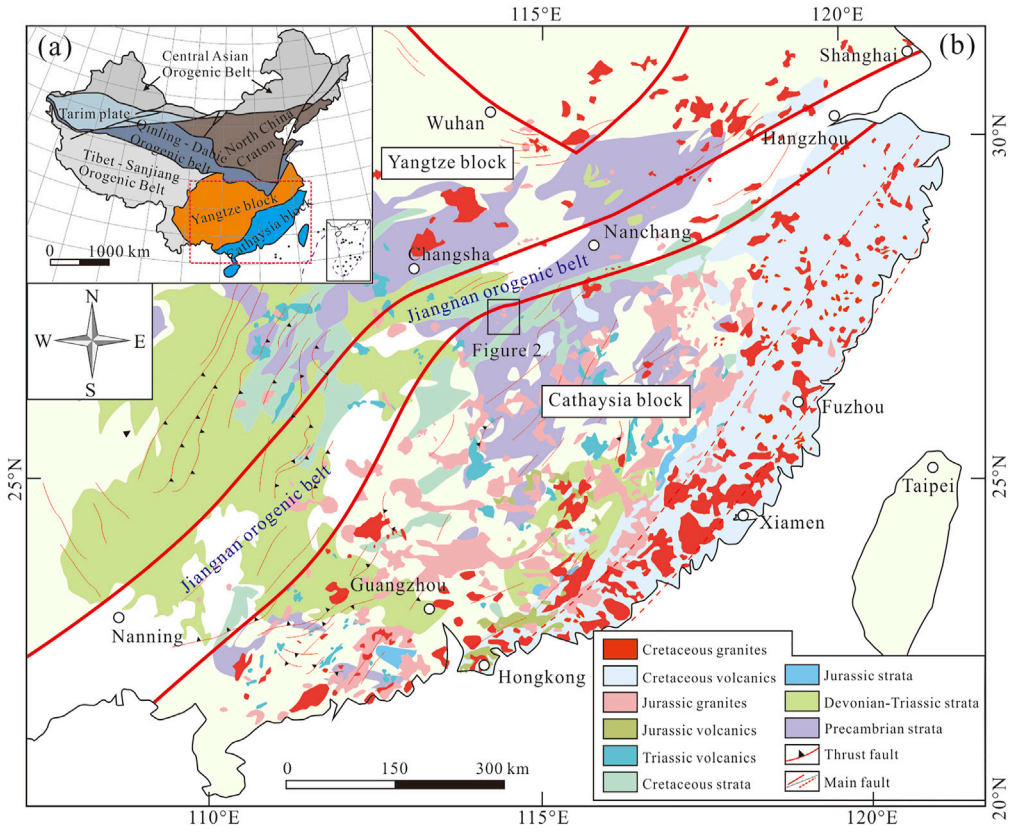

FIGURE 1
(A) Structure outline map of China (modified from Zhao and Guo, 2012); **(B)** regional geological map of South China (modified from He et al., 2010).

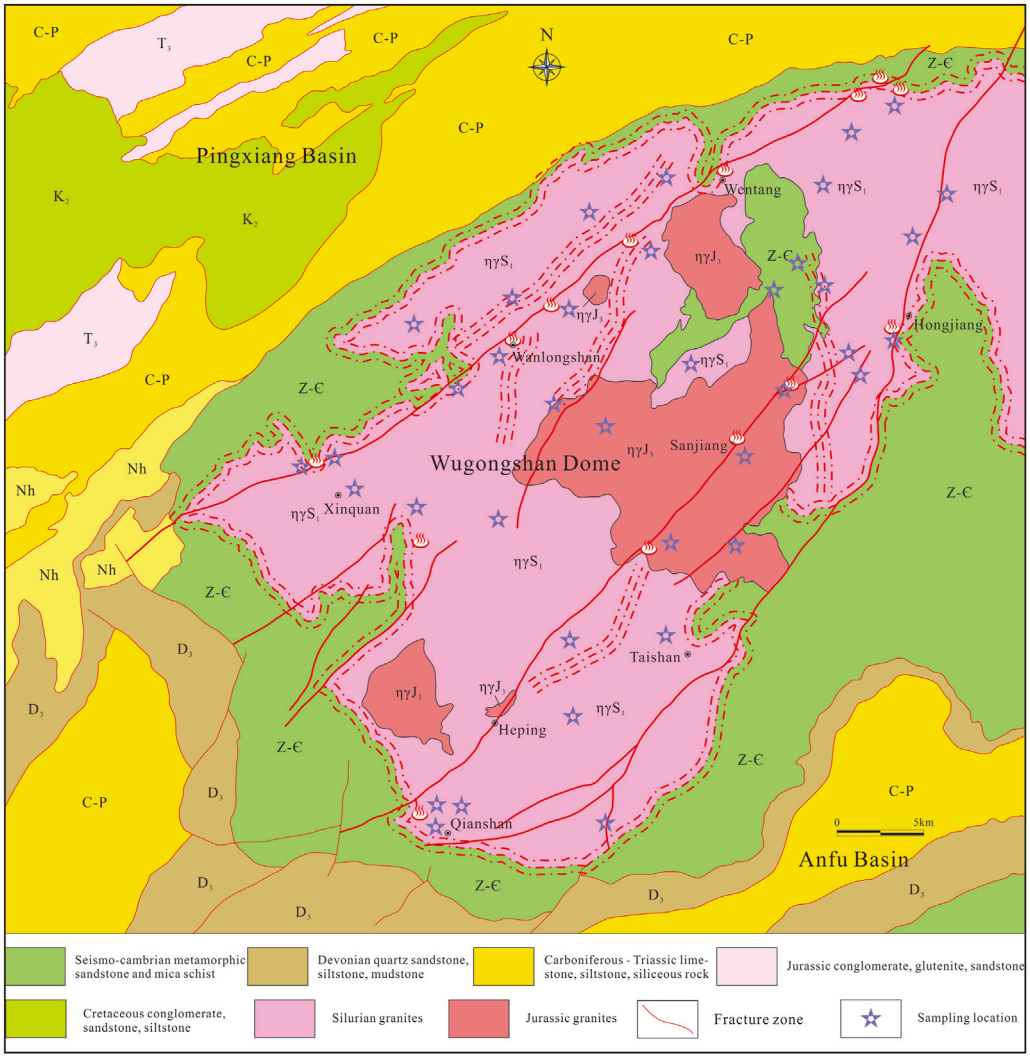

FIGURE 2
Geothermal geological map of the Wugongshan area (modified from Shu et al., 2000).

prerequisite for the development and utilization of geothermal resources.

The study of thermophysical parameters is of great significance for the analysis of geothermal genesis. The parameters are indispensable for research into temperature distribution and heat transfer in the surface and interior of the earth. However, due to the lack of geological research, the potential of the geothermal energy resource in the Wugongshan area is undeveloped at present. Therefore, 85 rock samples, covering typical strata and magmatic rocks, were collected from the surface and boreholes in the Wugongshan area for estimating thermophysical parameters, including thermal conductivity, thermal diffusivity, specific heat capacity, density and radioactive heat generation rate, and analyzing the distribution characteristics of thermophysical parameters of rocks in different strata. This study provides important basic data for geothermal genesis and future exploration and utilization of geothermal resources in the Wugongshan area.

2 Regional geological setting

The Wugongshan area is located in the middle part of the Jiangnan orogenic belt in South China, on the south side of the convergence belt of the Yangtze Block and the Cathaysia Block, and belongs to the middle Jiangxi tectonic collision belt in the northern margin of the Cathaysia Block (Figure 1). From the Neoproterozoic to the present, it has experienced the superimposed transformation of multiple tectonic movements, such as active continental margin, plate collision and uplift, and intra-continental orogeny, and the structural traces of different levels are interwoven, showing the general characteristics of complex orogenic belts (Faure et al., 1996; Li, 1998; Li et al., 2008; Li et al., 2009). There exist both the compressive tectonic system related to the subduction-collision orogenic belt and the multi-level and multi-sequence extension-slip overburden tectonic system caused by the post-orogenic extension (Sun et al., 1994; 1997; Faure et al., 1996; Shu et al., 1998; 2000; Lou et al., 2002; 2005). The Wugongshan area is an ellipse with a long axis of about 70 km and a short axis of about

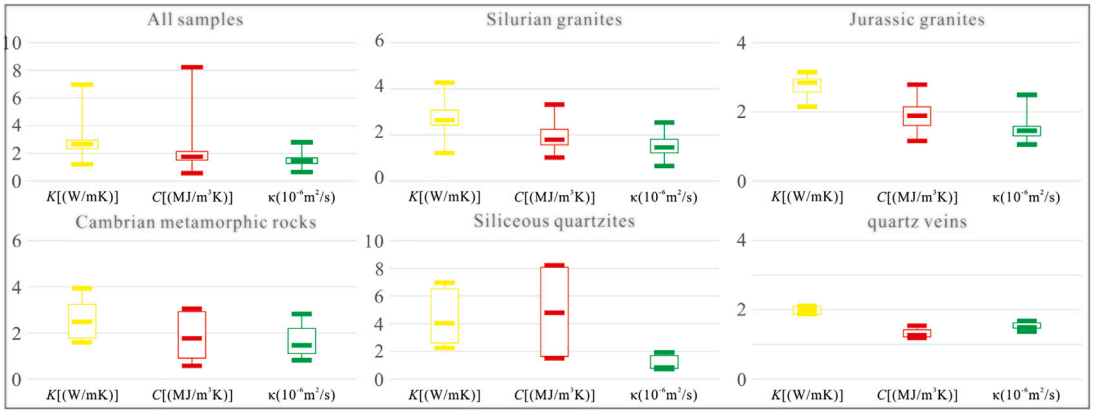

FIGURE 3
Boxplot of thermophysical parameters in the Wugongshan area (K, thermal conductivity; *C*, specific heat capacity; κ, thermal diffusivity).

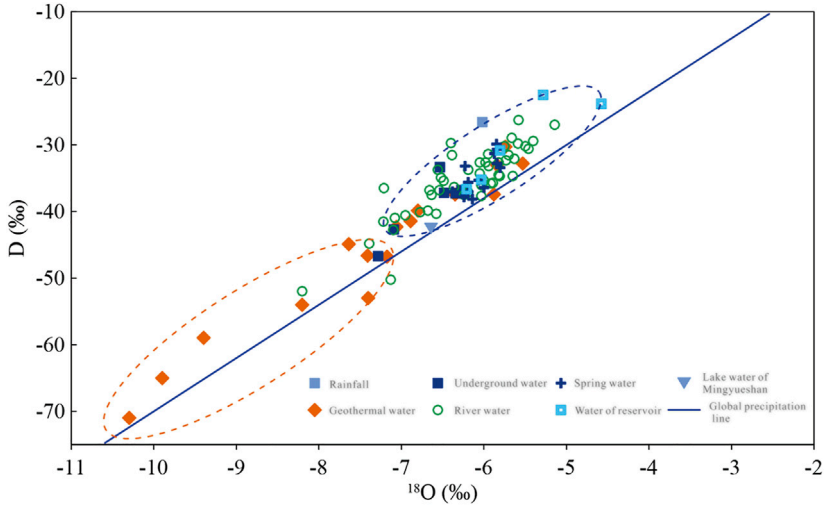

FIGURE 4
Histograms of thermal conductivities in the Wugongshan area.

30 km, covering an area of about 1.5 × 10^3 km^2. Trending from the northeast to the southwest, the ratio of the long and short axes is about 2: 1. The axis is located in the Qianshan–Sanjiang–Hongjiang area, which is Jurassic granite (Figure 2).

The basement strata in the Wugongshan area are the Sinian and Cambrian strata. The Sinian strata are distributed in the southern and western part of Wugongshan, mainly consisting of the Bali Formation and the Laohutang Formation (Faure et al., 1996; Shu et al., 1998). The Bali Formation (Z_2b) is mainly composed of garnet mica schist, garnet biotite quartz schist, and quartz schist. The Laohutang Formation (Z_2lh) has three layers. The bottom layer is gray–white medium-thin bedded siliceous rock, the middle layer is garnet biotite granitic rock assemblage, and the upper layer is light gray, gray–white medium–thin bedded banded siliceous rock. The Cambrian strata are distributed in the west, east, and northeast of Wugongshan, with the Niujiaohe Formation, Gaotan Formation, and Wentang Formation. The Niujiaohe Formation (ϵ_1n) is interbedded with didolomite quartz schist and unequal grained feldspar quartz complex sandstone. The Gaotan Formation (ϵ_2gt) is composed of garnet schist, plagioclase schist, etc. The Wentang Formation (ϵwt) is a globally disordered and locally ordered medium–deep metamorphic rock series with marbling limestone. The Mesozoic and Cenozoic strata are rarely exposed, and the Quaternary strata are distributed in the banks of the Lushui and Yuanshui and their tributaries and the mountain valleys, forming terraces at all levels of the floodplains and river valleys (Zhang et al., 2022).

Since the Neoproterozoic, the Wugongshan area has undergone three tectonic-magmatic evolution stages: Early Paleozoic, Middle Triassic, and Late Triassic to Early Cretaceous (Ren, 1991; Li, 1998; Faure et al., 2009; Chen et al., 2010; Charvet, 2013). From the Late Triassic to the Early Cretaceous, the Yanshanian extended to the intense intercontinental orogeny period, and the Wugongshan granite dome structure was formed in this area, composed of overlying strata, core and

10.3389/fenvs.2023.1112143

TABLE 1 Thermophysical parameters of rocks in the Wugongshan area.

Serial number	Sample number	Longitude	Latitude	Depth	Period	Lithology	Th (μg/g)	U (μg/g)	K (%)	Density (g/cm^3)	Radioactive heat generation rate (μW/m^3)	Thermal conductivity (W/mK)	Specific heat (MJ/m^{3}K)	Thermal diffusivity (10^{-6} m^2/s)
1	CJZK05-1	114°07′06″	27°21′29″	1157.19	Silurian	Granite	17.4	6.57	3.73	2.661	3.19	2.775	1.451	1.912
2	CJZK05-2	114°07′06″	27°21′29″	1037.45	Silurian	Granite	22	7.64	3.11	2.674	3.74	2.281	1.574	1.449
3	CJZK05-3	114°07′06″	27°21′29″	930.12	Silurian	Granite	30.4	6.56	3.48	2.675	4.07	3.302	3.310	0.998
4	CJZK05-4	114°07′06″	27°21′29″	852.39	Silurian	Granite	19.2	5.29	3.34	2.678	2.98	1.215	1.567	0.775
5	DJFZK02-1	114°22′32.8″	27°32′25.9″	224.25	Cambrian	Biotite schist	24.6	4.25	3.74	2.784	3.24	1.590	0.566	2.812
6	DJFZK02-2	114°22′32.8″	27°32′25.9″	495.45		Siliceous quartzite	7.61	1.05	2.19	2.600	0.96	2.831	1.491	1.899
7	DJFZK02-3	114°22′32.8″	27°32′25.9″	704.56	Silurian	Granite	23	2.38	3.00	2.680	2.46	2.342	1.239	1.890
8	DJFZK02-4	114°22′32.8″	27°32′25.9″	839.75	Silurian	Granite	27.7	2.24	3.08	2.655	2.74	3.230	2.988	1.081
9	DJFZK02-5	114°22′32.8″	27°32′25.9″	977.57	Silurian	Granite	14	6.45	2.10	2.759	2.89	2.559	1.693	1.512
10	DJFZK01-1	114°22′14″	27°31′60″	800.37	Silurian	Granite	27.3	2.53	2.58	2.664	2.74	2.715	1.496	1.815
11	DJFZK01-2	114°22′14″	27°31′60″	641.51	Silurian	Granite	24	2.85	3.05	2.662	2.64	2.592	1.269	2.043
12	DJFZK01-3	114°22′14″	27°31′60″	473.34	Silurian	Granite	9.02	1.52	1.70	2.655	1.16	1.965	3.004	0.654
13	DJFZK01-5	114°22′14″	27°31′60″	345.28	Cambrian	Metamorphic quartz sandstone	10.6	3.29	8.42	2.635	2.31	2.554	1.759	1.452
14	DJFZK01-6	114°22′14″	27°31′60″	250.64	Cambrian	Biotite schist	12.1	2.39	2.15	2.751	1.68	3.921	2.801	1.400
15	SJZK01-1	114°17′50″	27°33′23″	242.72	Jurassic	Granite	31	7.07	5.05	2.628	4.32	2.147	1.973	1.088
16	SJZK01-3	114°17′50″	27°33′23″	517.38	Jurassic	Granite	29.7	8.04	4.22	2.634	4.41	2.887	1.159	2.491
17	SJZK01-5	114°17′50″	27°33′23″	869.68	Jurassic	Granite	27.3	11.13	3.89	2.619	4.96	2.841	1.655	1.717
18	SJZK01-6	114°17′50″	27°33′23″	1026.86	Jurassic	Granite	31.6	17.51	4.21	2.628	6.90	2.948	2.783	1.059
19	SJZK01-7	114°17′50″	27°33′23″	1168.68	Jurassic	Granite	51.1	21.09	3.56	2.669	9.18	2.365	1.272	1.859
20	SJZK01-9	114°17′50″	27°33′23″	1443.41	Jurassic	Granite	70.6	14.39	3.65	2.659	8.79	2.654	1.748	1.518
21	XQZK11-1	114°03′32″	27°32′06″	332.35	Silurian	Granite	1.4	8.77	3.54	2.642	2.63	3.077	2.301	1.337
22	XQZK11-2	114°03′32″	27°32′06″	438.7	Silurian	Granite	21.4	3.75	3.12	2.657	2.69	2.943	1.744	1.688
23	XQZK11-3	114°03′32″	27°32′06″	558.87	Silurian	Granite	12.3	2.76	4.38	2.742	2.00	2.784	1.659	1.678
24	XQZK11-4	114°03′32″	27°32′06″	658.96	Silurian	Granite	23.2	3.36	2.93	2.744	2.79	4.267	1.979	2.156

(Continued on following page)

TABLE 1 (*Continued*) Thermophysical parameters of rocks in the Wugongshan area.

Serial number	Sample number	Longitude	Latitude	Depth	Period	Lithology	Th (μg/g)	U (μg/g)	K (%)	Density (g/cm^3)	Radioactive heat generation rate (μW/m^3)	Thermal conductivity (W/mK)	Specific heat (MJ/m^{3}K)	Thermal diffusivity (10^{-6} m^2/s)
25	XQZK11-6	114°03′32″	27°32′06″	869.1		Siliceous quartzite	4.97	1.06	2.16	2.625	0.80	5.215	6.417	0.813
26	XQZK11-7	114°03′32″	27°32′06″	963.08	Silurian	Granite	2.27	5.19	2.54	2.740	1.76	2.063	3.023	0.682
27	XQZK12-1	114°41′42″	27°40′44.8″	1599.64	Silurian	Granite	12	4.2	2.88	2.671	2.15	2.466	2.835	0.870
28	XQZK12-3	114°41′42″	27°40′44.8″	1398.32	Silurian	Granite	8.64	4.49	2.75	2.657	1.98	2.512	2.043	1.230
29	XQZK12-4	114°41′42″	27°40′44.8″	1262.89	Silurian	Granite	8.99	8.05	4.07	2.649	3.01	2.107	1.964	1.073
30	XQZK12-5	114°41′42″	27°40′44.8″	1133.07	Silurian	Granite	8.42	7.68	3.89	2.637	2.85	3.224	1.616	1.995
31	CJZK06-1	114°07′13.2″	27°21′22.5″	179.7	Silurian	Granite	16.2	4.51	4.00	2.649	2.61	2.764	1.679	1.646
32	CJZK06-2	114°07′13.2″	27°21′22.5″	443.26	Silurian	Granite	15.5	4.85	3.11	2.686	2.60	2.974	1.888	1.575
33	CJZK06-3	114°07′13.2″	27°21′22.5″	647.9	Silurian	Granite	12.6	5.33	3.81	2.658	2.56	3.159	1.580	1.999
34	CJZK06-4	114°07′13.2″	27°21′22.5″	755.4	Silurian	Granite	12.6	7.4	4.11	2.681	3.14	3.298	2.272	1.452
35	XQZK13-1	114°06′19.5″	27°33′31.1″	115.07	Cambrian	Metamorphic quartz sandstone	25.9	4.06	4.87	2.808	3.42	2.476	3.041	0.814
36	XQZK13-2	114°06′19.5″	27°33′31.1″	248.4	Silurian	Granite	14.8	1.61	2.49	2.721	1.68	2.616	1.031	2.537
37	XQZK13-3	114°06′19.5″	27°33′31.1″	368.41		Siliceous quartzite	0.05	0.01	0.12	2.623	0.02	6.959	8.214	0.847
38	XQZK13-4	114°06′19.5″	27°33′31.1″	500.99	Silurian	Granite	10.6	1.82	2.19	2.631	1.37	2.435	1.021	2.385
39	XQZK13-6	114°06′19.5″	27°33′31.1″	757.53		Siliceous quartzite	0.31	0.1	0.56	2.535	0.09	6.354	8.016	0.793
40	XQZK13-7	114°06′19.5″	27°33′31.1″	870.8		Siliceous quartzite	0.53	0.15	0.18	2.723	0.09	2.238	3.145	0.711
41	G202104	114°7′26″	27°33′59″	Surface		Quartz vein	0.081	0.041	0.04	2.650	0.02	2.023	1.245	1.625
42	G202108	114°10′16″	27°36′15″	Surface		Quartz vein	7.55	0.87	1.65	2.570	0.86	1.987	1.183	1.680
43	G202110	114°17′20″	27°41′28″	Surface		Quartz vein	1.12	0.35	0.46	2.620	0.20	2.114	1.541	1.372
44	G202113	114°17′57″	27°32′49″	Surface		Quartz vein	0.39	1.26	0.24	2.540	0.35	1.874	1.268	1.478
45	G202115	114°18′15″	27°33′6″	135.00	Jurassic	Granite	21.4	9.04	5.23	2.970	4.72	2.983	1.887	1.581
46	G202116	114°18′15″	27°33′6″	257.00	Jurassic	Granite	25.4	14.6	3.84	2.870	6.24	2.842	1.754	1.620
47	G202117	114°18′15″	27°33′6″	410.00	Jurassic	Granite	17.1	9.02	1.74	2.940	3.99	3.012	2.143	1.406

(Continued on following page)

10.3389/fenvs.2023.1112143

TABLE 1 (*Continued*) Thermophysical parameters of rocks in the Wugongshan area.

Serial number	Sample number	Longitude	Latitude	Depth	Period	Lithology	Th (μg/g)	U (μg/g)	K (%)	Density (g/cm^3)	Radioactive heat generation rate (μW/m^3)	Thermal conductivity (W/mK)	Specific heat (MJ/m^{3}K)	Thermal diffusivity (10^{-6} m^2/s)
48	G202118	114°18′15″	27°33′6″	490.00		Quartz vein	3.56	4.96	5.73	2.580	1.97	1.977	1.254	1.577
49	G202119	114°18′15″	27°33′6″	600.00	Jurassic	Granite	20.4	23.8	3.68	2.970	8.67	2.879	2.012	1.431
50	G202120	114°18′15″	27°33′6″	770.00	Jurassic	Granite	22.5	5.20	3.54	2.890	3.45	3.146	2.312	1.361
51	G202121	114°18′15″	27°33′6″	850.00	Jurassic	Granite	34.9	14.8	4.19	2.870	7.02	2.887	2.014	1.433
52	G202122	114°18′15″	27°33′6″	950.00	Jurassic	Granite	24.6	8.79	3.46	2.880	4.57	2.796	1.877	1.490
53	G202123	114°18′15″	27°33′6″	1060.00	Jurassic	Granite	23.6	24.9	4.02	2.780	8.65	2.987	2.056	1.453
54	G202124	114°18′15″	27°33′6″	1170.00	Jurassic	Granite	27.1	6.68	2.77	2.950	4.21	2.784	1.645	1.692
55	G202125	114°18′15″	27°33′6″	1275.00	Jurassic	Granite	24.4	11.0	4.54	2.970	5.43	3.124	2.147	1.455
56	G202126	114°18′15″	27°33′6″	1365.00	Jurassic	Granite	24.5	8.24	1.42	3.010	4.39	2.945	2.256	1.305
57	G202131	114°18′27″	27°35′29″	Surface		Siliceous quartzite	0.25	1.36	0.26	2.740	0.40	2.745	1.689	1.625
58	G202132	114°18′27″	27°35′29″	Surface		Quartz vein	0.18	0.20	0.08	2.680	0.07	2.112	1.421	1.486
59	G202133	114°18′27″	27°35′29″	Surface	Jurassic	Granite	6.76	15.1	2.17	2.680	4.51	2.887	1.874	1.541
60	G202139	114°23′13″	27°37′46″	Surface		Quartz vein	0.13	0.42	0.02	2.560	0.11	1.978	1.345	1.471
61	G202140	114°23′52″	27°37′55″	Surface		Quartz vein	0.070	0.10	0.04	2.610	0.03	1.874	1.221	1.535
62	G202142	114°6′19″	27°33′31″	310.00	Silurian	Granite	10.9	10.0	1.83	2.940	3.81	3.112	2.247	1.385
63	G202143	114°7′33″	27°21′12″	1090.00	Silurian	Granite	6.25	1.38	1.52	2.540	0.87	2.487	1.438	1.729
64	G202144	114°7′33″	27°21′12″	1050.00	Silurian	Granite	17.1	6.14	3.53	2.870	3.29	3.114	2.336	1.333
65	G202145	114°7′33″	27°21′12″	1250.00	Silurian	Granite	15.6	6.15	3.03	2.940	3.21	3.078	2.038	1.510
66	WGS06004	114°13′44″	27°36′38″	Surface	Silurian	Granite	15.4	8.81	3.00	2.740	3.67	2.570	1.758	1.462
67	WGS06006	114°08′197″	27°38′10″	Surface	Silurian	Granite	24.2	4.20	4.56	2.810	3.31	2.678	2.071	1.293
68	WGS06007	114°17′5″	27°40′6″	Surface	Jurassic	Granite	7.12	9.09	4.01	2.730	3.24	2.989	1.560	1.916
69	WGS06011	114°20′59.7″	27°31′18.9″	Surface	Silurian	Granite	22.5	2.79	3.56	2.750	2.66	2.525	1.791	1.410
70	WGS06012	114°15′38″	27°28′34.6″	Surface	Silurian	Granite	19.70	6.28	5.42	2.830	3.65	1.830	1.819	1.006
71	WGS06014	114°16′16.8″	27°30′56.2″	Surface	Jurassic	Granite	19.72	23.80	4.34	2.910	8.50	2.678	2.095	1.278
72	WGS06015	114°15′12.5″	27°31′10.9″	Surface	Jurassic	Granite	13.18	9.10	4.25	2.840	3.84	2.886	2.417	1.194

(Continued on following page)

10.3389/fenvs.2023.1112143

TABLE 1 (*Continued*) Thermophysical parameters of rocks in the Wugongshan area.

Serial number	Sample number	Longitude	Latitude	Depth	Period	Lithology	Th (μg/g)	U (μg/g)	K (%)	Density (g/cm^3)	Radioactive heat generation rate (μW/m^3)	Thermal conductivity (W/mK)	Specific heat (MJ/m^{3}K)	Thermal diffusivity (10^{-6} m^2/s)
73	WGS06017	114°11′35″	27°20′11.4″	Surface	Silurian	Granite	18.25	5.19	3.57	2.860	3.10	2.756	2.060	1.338
74	WGS06018	114°10′21.1″	27°24′53″	Surface	Jurassic	Granite	36.27	6.32	4.41	2.970	5.00	2.357	1.587	1.485
75	WGS06022	114°5′2″	27°30′56″	Surface	Silurian	Granite	15.97	2.54	4.68	2.880	2.34	2.574	1.573	1.636
76	WGS06023	114°10′38″	27°32′4″	Surface	Jurassic	Granite	39.22	2.78	3.02	2.790	3.83	2.216	1.494	1.483
77	WGS06024	114°9′35″	27°32′4″	Surface	Silurian	Granite	19.08	3.37	3.06	2.710	2.48	2.348	2.255	1.041
78	WGS06026	114°10′13″	27°39′35″	Surface	Silurian	Granite	20.47	5.10	3.20	2.780	3.12	2.309	1.501	1.538
79	WGS06027	114°17′44″	27°34′54″	Surface	Jurassic	Granite	8.83	32.48	2.99	2.730	9.34	2.650	2.144	1.236
80	WGS06030	114°15′20″	27°32′51″	Surface	Jurassic	Granite	10.83	6.48	4.03	2.670	2.76	2.255	1.607	1.403
81	WGS06032	114°10′36.3″	27°27′2″	Surface	Silurian	Granite	14.90	3.73	4.36	2.890	2.57	2.644	1.571	1.683
82	WGS06033	114°26′3.8″	27°39′4.4″	Surface	Silurian	Granite	13.50	3.21	3.51	2.740	2.12	2.441	1.086	2.248
83	WGS06034	114°23′0.1″	27°36′50.7″	Surface	Silurian	Granite	14.62	2.84	2.36	2.980	2.17	2.774	1.950	1.423
84	WGS06035	114°20′6″	27°34′21″	Surface	Jurassic	Granite	43.48	5.01	4.00	2.710	4.69	2.571	2.044	1.258
85	WGS06037	114°17′50.5″	27°38′50.3″	Surface	Jurassic	Granite	8.37	6.36	4.40	2.670	2.60	2.377	1.605	1.481

10.3389/fenvs.2023.1112143

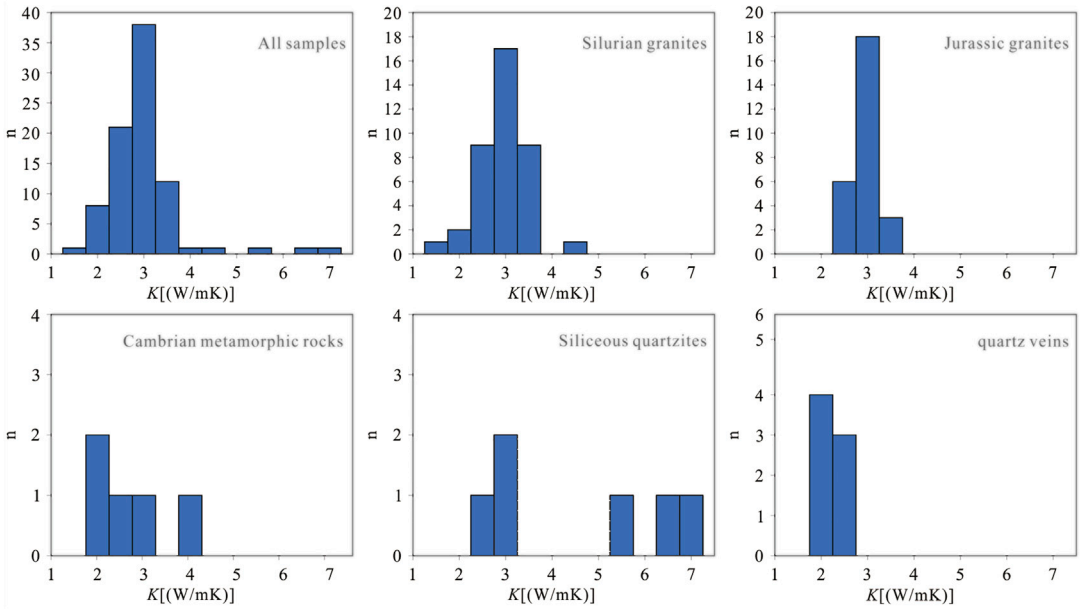

FIGURE 5
Superposition diagram of the geothermal geological map with thermal conductivity isolines.

detachment fault zones. The overlying strata of the Wugongshan granite dome structure are composed of Devonian–Triassic metamorphic-sedimentary strata. A series of single oblique overburden sheets are found on the north and south sides of the dome, mainly related to the Mesozoic extensional slip. The faults in the Wugongshan area mainly trend to the northeast, and the secondary faults are NNE-trending and NW-trending. The two groups of faults share the hanging-wall position, and the rocks are very broken, easily forming a regional thermal anomaly output channel. The asthenospheric uplift in this area forms the convex isothermal surface in the region, and the shallow rock mass is affected by the decay heat of radioactive elements in the late deep intrusive rock mass and the deep heat source by fault transmission-conduction, forming geothermal resources.

Strong magmatic activities in the Wugongshan area created the Siluric-Jurassic granites. The lithology, structural structure, mineral association, and other aspects indicate they are complex rocks with homologous magmatic evolution characteristics. Silurian granites are distributed in Nanmiao Town, Taishan Town, Wentang Town, Hongjiang Town, Xinquan Town, Qianshan Town, and other places in Wugongshan, with a NE direction. The lithology is mainly biotite monzogranite, granodiorite, and monzogranite, and its component minerals are plagioclase, potassium feldspar, biotite, amphibole, and a small amount of quartz. The rocks were generally transformed by the late tectonic orogeny, and the minerals were oriented. Gneiss-like structures were developed, and gneiss was developed at the edge of the rock mass. Jurassic granites are distributed in the areas of Mingyueshan, Sanjiang, Hukeng, and Xiaojialing at the core of Wugongshan (Figure 2). They are mostly elliptic and irregular in plane and generally show a NE direction. The lithology is dominated by monzogranite and biotite granite, and its constituent minerals are potassium feldspar, plagioclase, quartz, biotite, and a small amount of Muscovite. The rocks have a porphyritic granitic structure (Faure et al., 2009; Zhang et al., 2022).

The geothermal fields in the Wugongshan area show several obvious characteristics: 1) hot springs mostly occur in the fracture zone or the intersection of two groups of faults with different directions. 2) The water is heated by deep circulation of groundwater, and there is no special additional heat source such as modern volcanic heat source or magmatic heat source in the shallow part. 3) The permeability of the rock mass is poor, and the water is mainly guided by fractures and fracture zones. Hot water gushes to the surface or shallows along the deep fault zone. 4) Local thermal anomalies are often formed near the hot water main stream zone, and the geothermal gradient in the center of the anomaly is more than 2–3 times higher than the normal value (Bai et al., 2021a; Bai et al., 2021b).

3 Sample collection and experimental methods

Based on a systematic field geological survey, a total of 85 samples of Cambrian metamorphic rocks, Silurian granite, Jurassic granite, siliceous quartzite, and quartz vein were collected from the surface and boreholes in the Wugongshan area. The locations of sampling points are shown in Figure 2.

The density, thermal conductivity, specific heat, and thermal diffusion of the samples were determined in the Laboratory of Rock Thermophysical and Geothermal Measurement of the Key Laboratory of Paleogeomagnetism and Paleostructure Reconstruction of the Ministry of Natural Resources. The analytical instrument was a thermal conductivity meter based on transient planar heat source technology (TPS) for thermal conductivity, thermal diffusion, and specific heat capacity manufactured by Hot Disk, Sweden. The instrument can be used to measure the thermophysical properties of various rock samples, such as thermal conductivity (range: 0.005–500 W/mk), specific heat

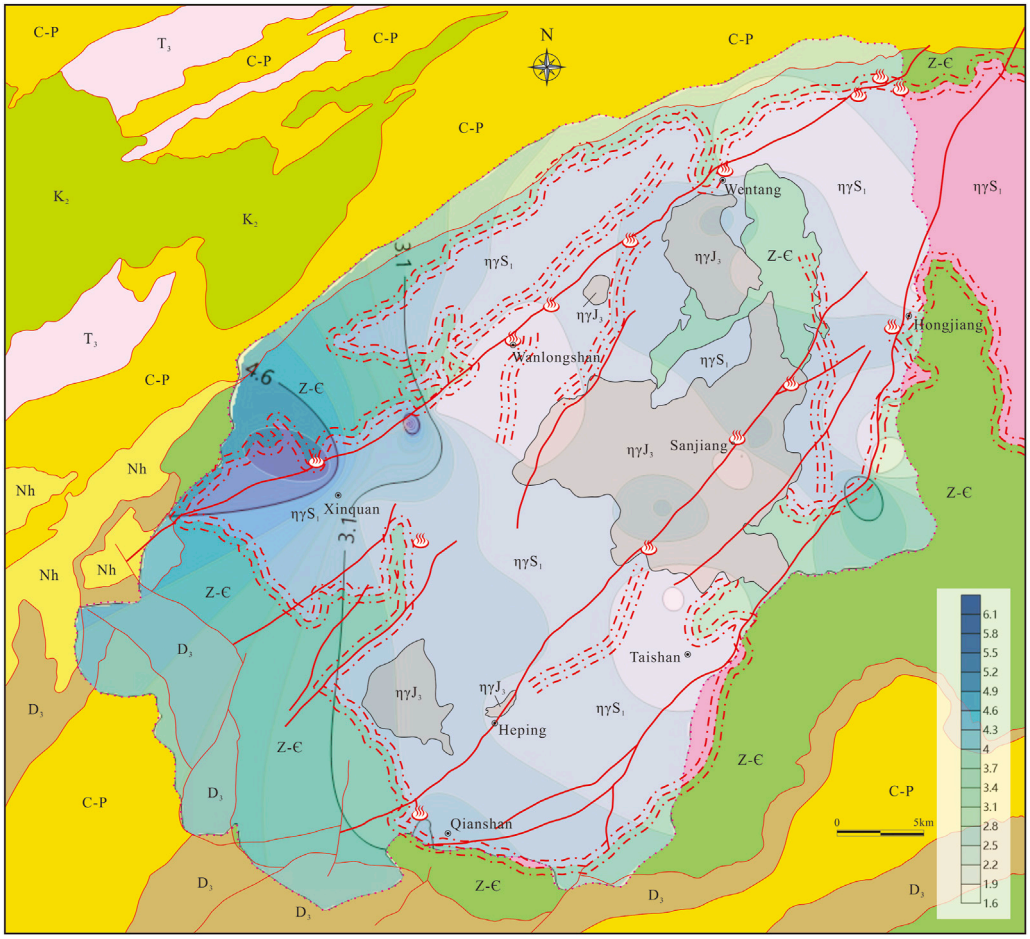

FIGURE 6
Histograms of specific heat capacities in the Wugongshan area.

capacity (temperature range: 10 K–10000 K), and thermal diffusibility with high accuracy (±3%) (Gustafsson, 1991). The experimental principle was the transient plane source (TPS) method (Gustavsson et al., 1994; Gustavsson and Gustavsson, 2005). The core component of the method was a probe with a spiral structure, which was etched into a 10 (±2)-μm-thick metal sheet that was insulated with a 4–100-μm film. The probe was placed between two samples for testing (Sizov et al., 2016). During the test, a certain temperature rise was generated by the current passing through the probe, and the heat capacity of the probe was negligible. The heat of the probe diffuses to both sides of the sample at the same time, and the average temperature rise of the probe surface was accurately measured according to the resistance change of the metal sheet of the probe (Gustavsson et al., 1997; Mihiretie et al., 2016). The Hot Disk probe is both a heat source and a temperature sensor. The probe was connected to an automatic data system that included experimental operating software and analysis of the transient curves of the experimental results with corresponding temperature function models (Mihiretie et al., 2017). The test results are shown in Table 1.

The content of U, Th, and K in rock samples was tested in the laboratory of the Hebei Institute of the Regional Geological Survey. The K test instrument was an Axiosmax X-ray fluorescence spectrometer. An XSeries 2 plasma mass spectrometer was used for U and Th analysis. The test temperature was 26°C, and the humidity was 40%. The test accuracy was better than 5%. The radioactive heat generation rate (A) of rocks was calculated using the following formula (Rybach, 1976) (1), and the results are shown in Table 1.

$$A = 0.01\rho\left(9.52C_U + 2.56C_{Th} + 3.48C_K\right) \quad (1)$$

where A is the radioactive heat generation rate of rock (μW/m^3), ρ is the rock density (unit: g/cm^3), C_U, C_{Th}, and C_K are the content of radioactive elements U, Th and K, respectively, and the units are ($\times10^{-6}$), ($\times10^{-6}$), and (wt%), respectively.

4 Results

4.1 Rock density

According to the measured data, the average density of rock samples in the Wugongshan area is 2.70 g/cm^3. The average density of rocks in the region ranges from 2.80 g/cm^3 for Jurassic granite to 2.73 g/cm^3 for Silurian granite, 2.71 g/cm^3 for Cambrian metamorphic rocks, 2.64 g/cm^3 for siliceous quartzite, and 2.60 g/cm^3 for quartz vein.

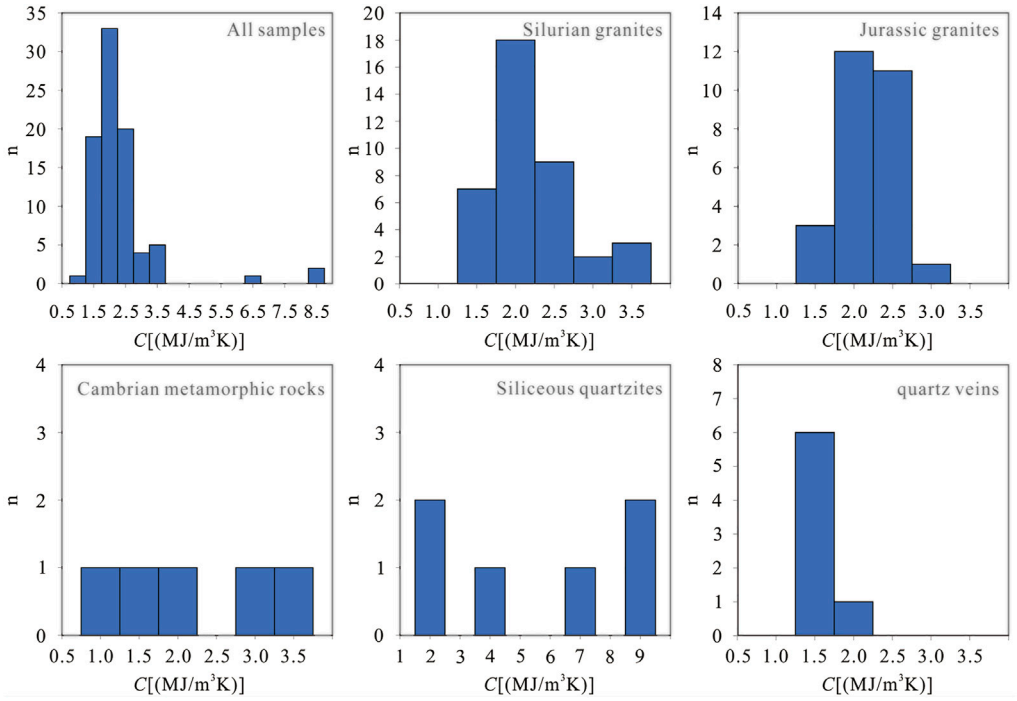

FIGURE 7
Superposition diagram of the geothermal geological map with specific heat capacity isolines.

4.2 Rock thermophysical parameters

The thermal conductivity of rock is the heat passing through a unit area in a unit of time when the temperature is reduced by one degree in a unit length along the direction of heat flow transfer, indicating the magnitude of the thermal conductivity of rock. The rocks in the area are grouped into five categories according to different ages and lithologies. Figure 3 shows the average thermal conductivity of the rocks in the area, which ranges from 1.995 to 4.390 W/mK. The average thermal conductivity in descending order is 4.390 W/mK for siliceous quartzite, 2.744 W/mK for Jurassic granite, 2.677 W/mK for Silurian granite, 2.504 W/mK for Cambrian strata, and 1.995 W/mK for quartz vein.

The specific heat capacity of rock is the heat capacity of a substance per unit mass; that is, the heat absorbed (or emitted) by a certain mass of a certain rock when its temperature rises (or falls) by one degree (Wang et al., 2015). The average specific heat of rocks in the area ranges from 1.318 to 4.829 MJ/m^{3}K (Table 1). The average specific heat value is 4.829 MJ/m^{3}K for siliceous quartzite, 1.905 MJ/m^{3}K for Silurian granite, 1.893 MJ/m^{3}K for Jurassic granite, 1.884 MJ/m^{3}K for Cambrian strata, and 1.318 MJ/m^{3}K for quartz vein.

The thermal diffusivity of rock is the product of the thermal conductivity divided by the density and specific heat capacity of rock; that is, k = K/ρC. Thermal diffusion of rock is a physical quantity that characterizes the temperature change rate of rock when the ambient temperature changes. According to Figure 3, the average thermal diffusion of rocks in the region ranges from 1.115 m^2/s to 1.611 m^2/s. The average thermal diffusivity is 1.611 m^2/s in Cambrian strata, 1.521 m^2/s in quartz vein, 1.506 m^2/s in Silurian granite, 1.490 m^2/s in Jurassic granite, and 1.115 m^2/s in siliceous quartzite.

4.3 Radioactive heat generation rate of rock

The decay heat generated by radioactive elements is an important power source that drives many deep tectonothermal processes in the earth's interior and is also one of the main heat sources of geothermal resources. As shown in Figure 3, the average radioactive heat generation rate of rocks in the Wugongshan area ranges from 0.24 to 5.49 μW/m^3. The radioactive heat generation rate is 5.49 μW/m^3 in Jurassic granite, 2.72 μW/m^3 in Silurian granite, 2.52 μW/m^3 in Cambrian strata, 0.39 μW/m^3 in siliceous quartzite, and 0.24 μW/m^3 in quartz vein.

5 Discussion

5.1 Hydrochemical analysis of geothermal groundwater

Hydrogen and oxygen are widely distributed in nature and are important components of groundwater. Groundwater originating from different sources has different stable isotopic compositions of hydrogen and oxygen (Liu et al., 2017). The variation of δD‰ in general atmospheric precipitation ranges from −160‰ to −30‰, and the variation of $\delta^{18}O$ ranges from −17‰ to +5‰. The relationship between δD and $\delta^{18}O$ is usually linear, and the δD and $\delta^{18}O$ of atmospheric precipitation in most areas are negative. In

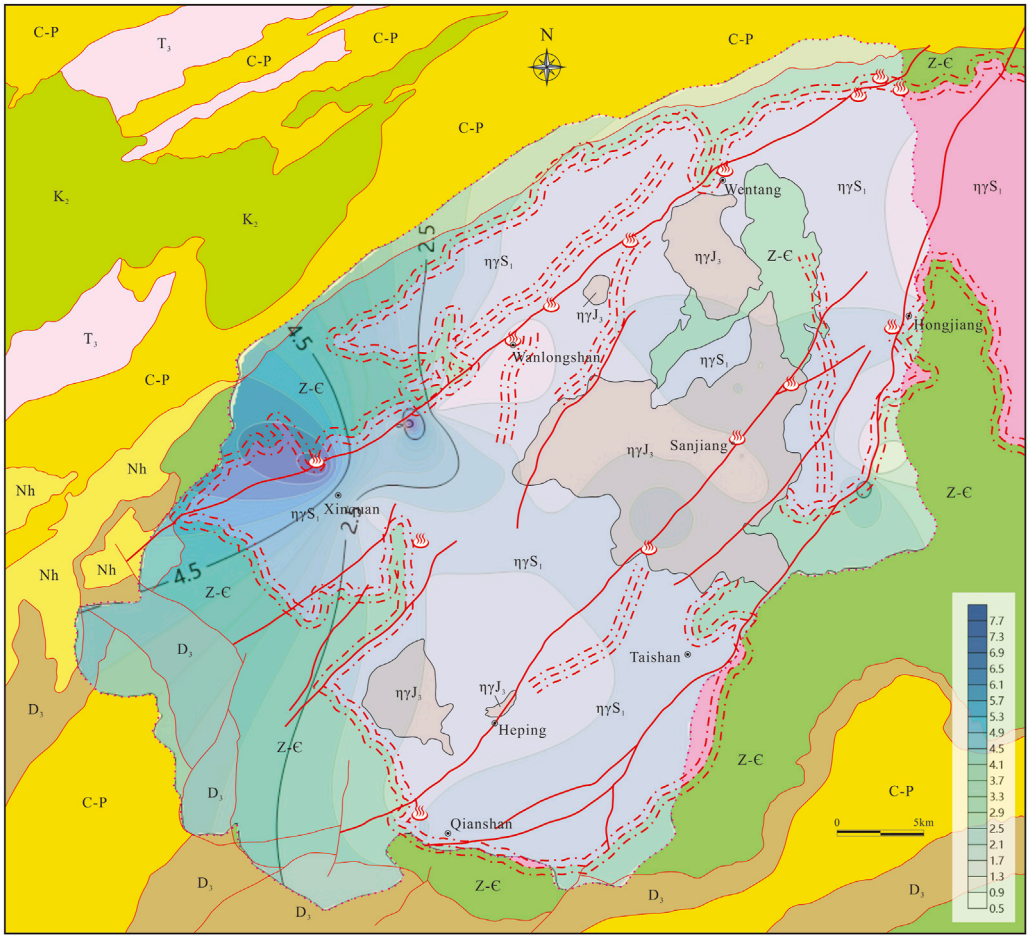

FIGURE 8
Histograms of thermal diffusivities in the Wugongshan area.

this study, samples of geothermal water, groundwater, spring water, and rainfall were analyzed, hydrogen and oxygen isotope tests were carried out (published separately), and the relationship diagram of $\delta^{18}O$ and δD of relevant water samples in the study area was obtained (Figure 4). The $\delta^{18}O$ and δD data of geothermal water, underground cold water, surface water, and other water samples in the Wugongshan area basically fell near the global atmospheric precipitation line. Almost all results are higher than the global atmospheric precipitation line, indicating that both geothermal water and cold water in the Wugongshan area are supplied by atmospheric precipitation, and water vapor recycling occurs in the area. The values of $\delta^{18}O$ and δD in most geothermal waters are lower than those of cold water, indicating that the hot water recharge rate in this area is higher, and hot springs are formed because the atmospheric precipitation is heated and rises to the surface after deep circulation.

5.2 Thermophysics analysis of rocks

Due to the significant difference in mineral composition, texture, and structure, the thermal conductivity of rock types differs. The thermal conductivity of the same type of rock will vary to some extent, due to the differences in mineral composition ratio and structure (Clauser, 2011; Jiang et al., 2016). Thermal conductivity increases with mineral content, and the thermal conductivity of rocks is high. In general, the thermal conductivity of rock increases with the increase of pressure, density, and humidity and decreases with the increase of temperature. The temperature and pressure of the upper crust have little effect on the thermal conductivity of rocks. As can be seen from Figure 5, the thermal conductivity data of the region are basically in a normal distribution pattern. The thermal conductivity data sets of Silurian and Jurassic granite are similar in distribution morphology, indicating that the rocks formed in the Silurian and Jurassic periods have similar thermal conductivity characteristics. The Cambrian strata and siliceous quartzite are relatively dispersed, which reflects the different thermal conductivities of rocks in different lithologies. The distribution map of the strata, rock outcropping areas, and thermal conductivity is shown in Figure 6. Rock samples with high thermal conductivities are mainly distributed in the western region. The lithology of this area is mainly Silurian monzogranite, siliceous quartzite, and Cambrian metamorphic rocks. The area of local high thermal conductivity in the study area is concentrated in two places.

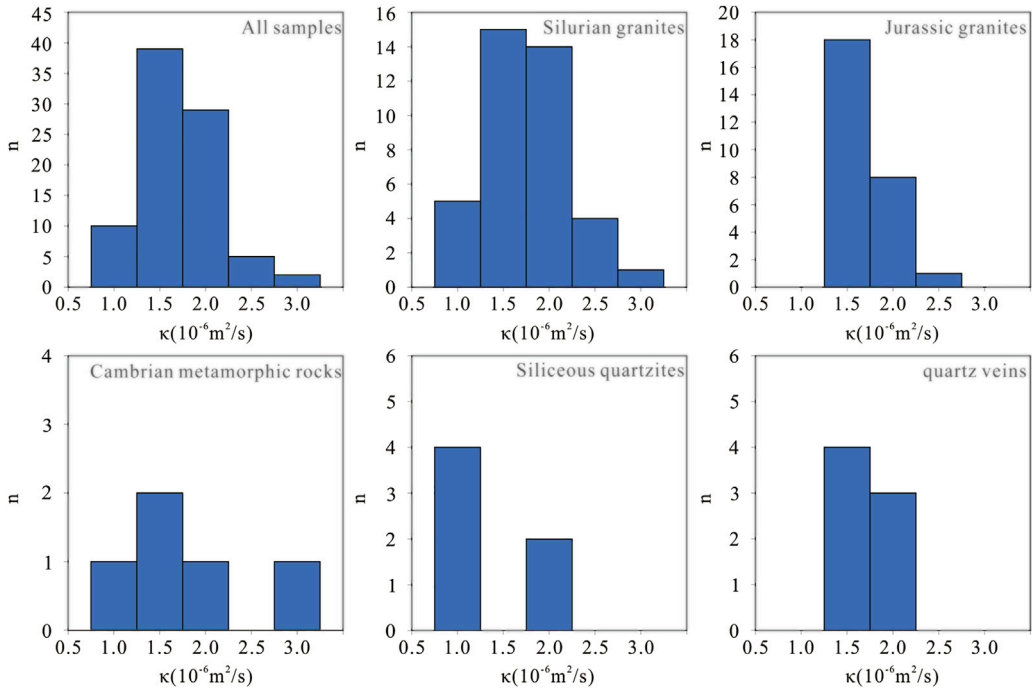

FIGURE 9
Superposition diagram of the geothermal geological map with thermal diffusivity isolines.

The thermal conductivity of the rocks in the Wugongshan area is mainly below 3.1 W/mK, and the characteristics of the thermal conductivity isoline are consistent with the lithologic characteristics of the geological map. The lithologic properties of the areas of high thermal conductivity are mainly siliceous quartzite and monzogranite.

Previous studies have revealed a negative correlation between the specific heat of rocks and quartz content at normal temperature (20°C), which means that the specific heat of rocks with large quartz content is relatively small (Jorand et al., 2015). The specific heat of rock increases with increasing temperature and porosity and decreases with increasing pressure (Xin et al., 2014; Miao and Zhou, 2017). However, there is no negative correlation between the specific heat of rocks and quartz content in the Wugongshan area. The maximum specific heat of siliceous quartzite is 4.829 MJ/m^{3}K, and the minimum specific heat of quartz vein is 1.318 MJ/m^{3}K. Figure 7 shows the frequency distribution of specific heats of different lithologies. Except for the Silurian and Jurassic granites, the frequency distribution of specific heats of other rocks varies and has a wide distribution range. Figure 8 shows that the high specific heat values in rock samples are mainly distributed in the western region, and the main lithology is siliceous quartzite. The distribution of local high specific heat in the study area is concentrated, and the distribution is consistent with the NE trending faults in the area. Combined with the thermal conductivity data, the siliceous quartzite is considered a good thermal conductive rock and a good thermal conductive channel.

Thermal diffusion of rock represents the ability of the rock's temperature to be uniform during heating or cooling. Heat diffuses rapidly and over a long distance in material with a high thermal diffusion rate, while in material with a low thermal diffusion rate, heat diffuses more slowly (Wang et al., 2015). As shown in Figure 8, the thermal diffusion rate of rock samples varies within a small range, but the siliceous quartzite has a relatively low thermal diffusion rate (1.115 m^2/s). The frequency distribution of thermal diffusivity in different lithologies is also shown in Figure 9. The distribution morphology of Silurian, Jurassic, and quartz veins are similar, indicating that these rocks have similar characteristics of thermal diffusivity. In Figure 10, the area of thermal diffusivity greater than 1.8×10^{-6} m^2/s is mainly distributed in the eastern part of the Wugongshan study area, while the thermal diffusivity values in the northern, southern, and central parts of the study area range from 1.3×10^{-6} m^2/s to 1.8×10^{-6} m^2/s. There was no obvious difference in thermal diffusivity among different lithologic blocks in the study area and no obvious zonation according to lithology. There is a linear relationship between thermal conductivity (K) and thermal diffusivity (κ) value in the area (Figure 11), and the correlation equation is

$$K = -0.3144\kappa + 3.2172 \quad (2)$$

Exploring the radioactive heat generation rate of rocks is one of the main investigations into the genetic mechanism of a geothermal system. It is important to investigate the contribution rate of radioactive decay heat to surface heat flow and clarify the thermal structure of the lithosphere to study the distribution of radioactive heat-generating elements in rocks (Zhao et al., 1995). The average radioactive heat generation rates measured in this paper are 5.49 μW/m^3 for Jurassic granites and 2.72 μW/m^3 for Silurian granites. The mean value of the global radioactive heat generation rate of granite is 2.1–2.5 μW/m^3 (Artemieva et al., 2017), and it is closely related to the age of granite. In Figure 12, the area with a high radioactive heat generation rate is consistent with the outcropping area of Jurassic granites. In previous

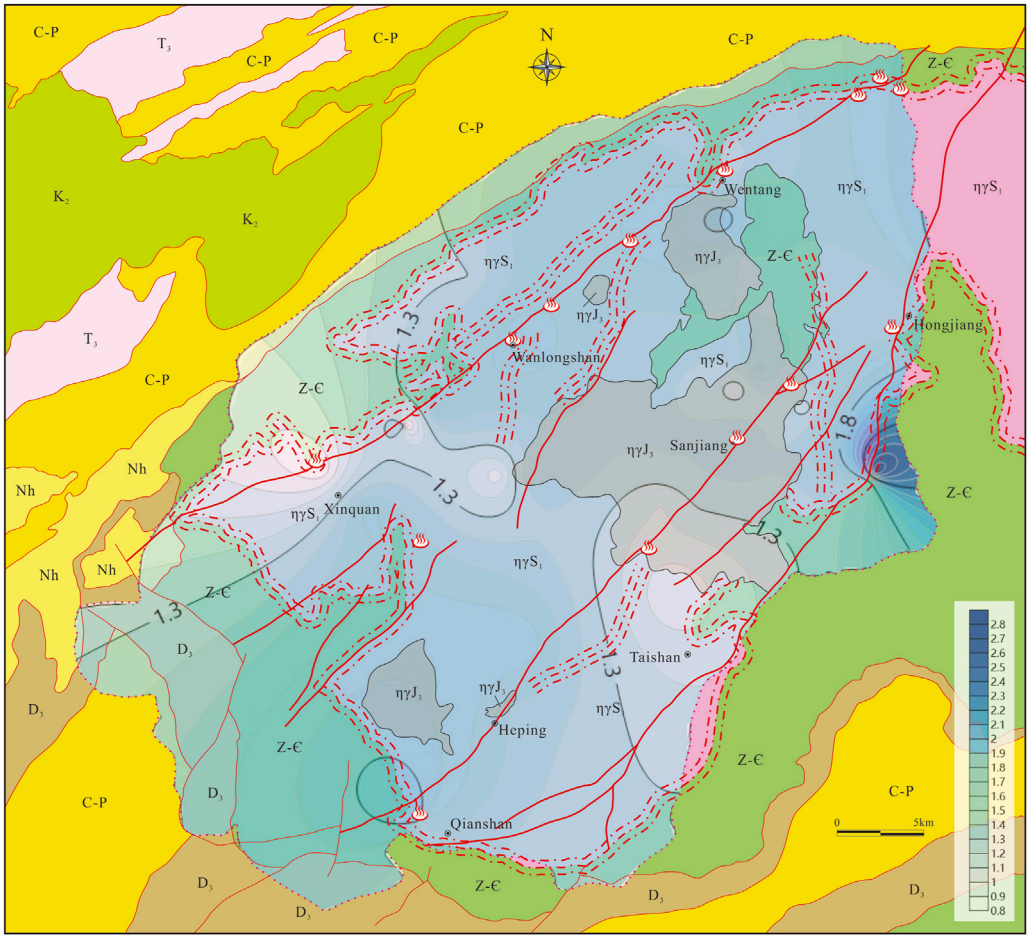

FIGURE 10
Coefficient curve of thermal conductivity and thermal diffusivity.

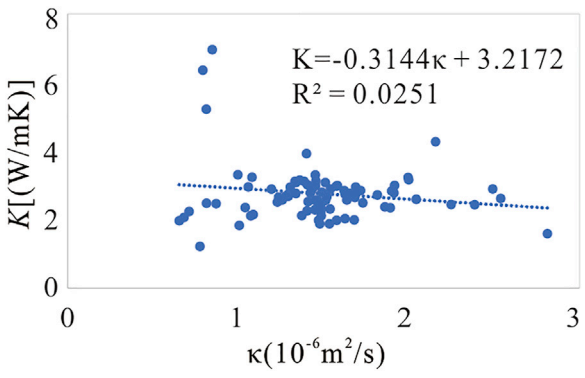

FIGURE 11
Superposition diagram of the geothermal geological map with radioactive heat generation rate isolines.

studies, the average value of terrestrial heat flow in the Wugongshan area was 90.4 mW/m^2 (internal data). This is much higher than the 62 mW/m^2 of the China mainland and the 65 mW/m^2 of the global continental average, indicating that the Wugongshan area is a region with a high heat flow value. The earth heat flow is the most accurate parameter to reflect a geothermal field. The high earth heat flow value in the study area indicates that this area has a high regional thermal background value and has good geothermal geological conditions for the development of geothermal fields. The average radiogenic heat generation rate of Jurassic granite is 5.49 μW/m^3, and the estimated radiogenic contribution heat flow is about 27.45–38.43 mW/m^2, accounting for 29.6%–41.4% of the average geothermal heat flow in the Wugongshan area. The Silurian granites do not exhibit strong anomalies. To sum up, the heat flow of granite radioactive elements in this area has a certain contribution to the heat source, but the contribution is limited, and it is not the main heat source of the Wugongshan area.

5.3 Genesis mechanism of geothermal resources

The heat sources of geothermal resources are mainly the following types: 1) partial melting layer in the crust (such as the Yangbajing geothermal field in Tibet (Dor and Zhao, 2000; Zhao

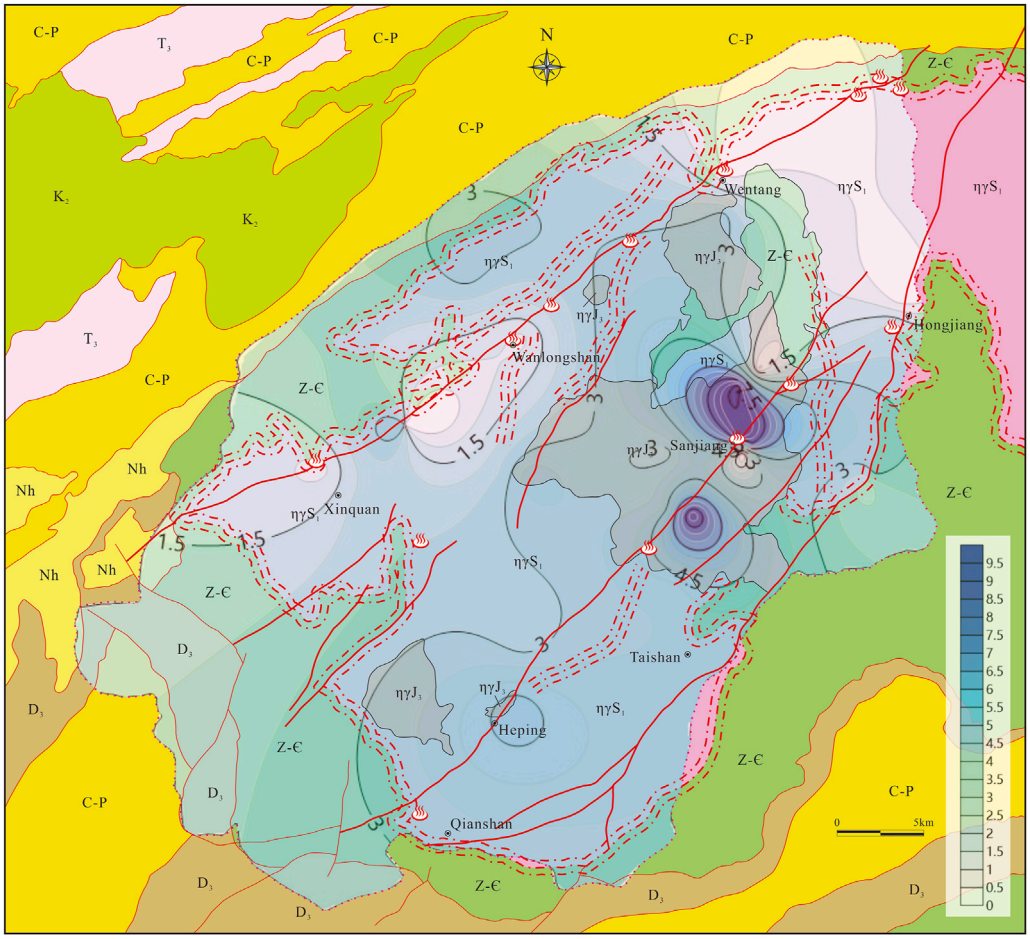

FIGURE 12
Relationship between $\delta^{18}O$ and δD in water samples in the Wugongshan area.

et al., 2001; Hu et al., 2022), the Gonghe-Guide geothermal field in Qinghai Province (Xue et al., 2013; Zhang et al., 2018a; Tang et al., 2020), the Guanzhong geothermal field in Shaanxi Province (Qin et al., 2005; Li et al., 2016; Luo et al., 2019), and the Tengchong geothermal field in Yunnan Province (Bai et al., 1994; Jiang et al., 2012; Zhao et al., 2012; Long et al., 2021)). 2) Cenozoic volcanic waste heat (the Changbaishan geothermal (Jiang et al., 2016; Zhao et al., 2017) and the Tengchong geothermal field (Zhao et al., 2012; Long et al., 2021)). 3) Deep rift geothermal (the Gulu and Yangying volcano-geothermal area, South Tibet (Zhang et al., 2017), the Wudalianchi geothermal field (Shao and Zhang, 2008), the Zhangzhou geothermal field (Lin et al., 2020), and the Okari geothermal field in Kenya (John et al., 2005; Zhang et al., 2018b)). 4) Heat generation by radioactive elements (the Ningdu geothermal in Jiangxi Province (Liu et al., 2020) and the Fogang geothermal field in Guangdong Province (Wang et al., 2015)). 5) Fault friction heat generation (the Yangshan geothermal field in Nanjing (Wu et al., 2021), the Western Sichuan geothermal field (Qu et al., 2019), and the Yanchihe hot spring in western Hubei (Xia, 1995)).

The Xinquan–Wentang fault and the Heping–Sanjiang fault were formed in the Yanshanian period, which controlled the Wanlongshan, Wentang, Wenjia, Sanjiang, Tangjiashan, and other geothermal fields. The value of helium gas in these fields is zero, which indicates that the heat source is crustal heat. According to the thermophysical parameters, the Silurian and Jurassic granites have higher thermal conductivity and specific heat, which are conducive to the accumulation and propagation of heat. Thus, the heat source in the Wugongshan area is mainly from the geothermal source in the deep crust. The siliceous quartzite in the fracture zone is developed and thick, which is conducive to conducting the deep heat to the shallow and surface areas. The geothermal energy collects heat and transfers heat in the granite near the fault zone, and the Xinquan–Wentang fault and Heping–Sanjiang fault are important thermal conductive and heat control structures in this area.

Due to the action of gravity, the surface atmospheric normal temperature precipitation seeps down along the rock fracture structures or joint fracture zones and gradually increases its temperature initially within the range of normal geothermal gradient, forming water that is warmer than the normal temperature. When the dispersed flow gathers near the heat-controlled and water-controlled fault (the northeast fault of the region), it basically presents zonal and linear runoff along the

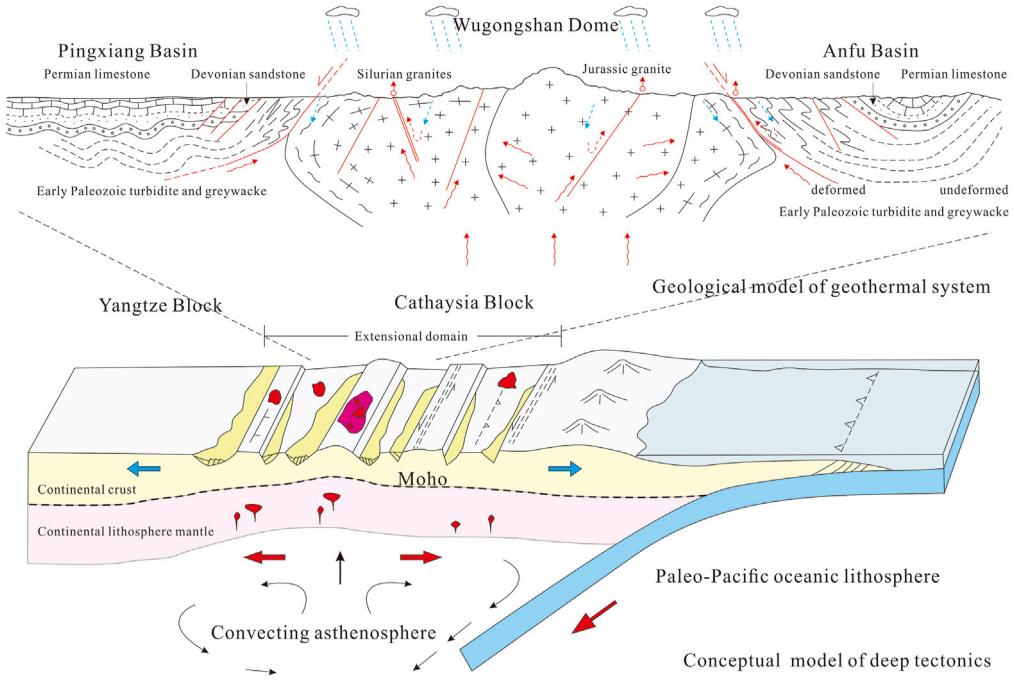

FIGURE 13
Genetic model map of geothermal resources in the Wugongshan area (modified from Shu et al., 1998; Li et al., 2019).

fault zone. Because the heat-controlled and water-controlled fault cuts deep into the crust, the siliceous quartzite in the fault zone conducts the heat in the deep crust upward and transfers and gathers heat in the shallow granite, thus forming a geothermal anomaly zone with sharply rising temperature. Geothermal water with a sharply rising temperature is formed by the heat absorbed by runoff in the anomaly zone when it encounters the water-blocking (isolation) structural plane (usually NEE-trending or NNW trending in this region) diagonally intersected with the heat-controlled and water-controlled fault. Because the geothermal water with a rising temperature has a lower density than the permeable normal water, the geothermal water floats up while the normal water permeates down (Figure 13). Under the effect of gully cutting, when there are water-conducted structures, geothermal water quickly rises along the water-conducted structure and overflows to the surface, forming hydrothermal geothermal resources.

6 Conclusion

This study analyzes the source, transport, and storage of geothermal resources to explain geothermal genesis. In the Wugongshan area, the thermophysical parameters of 85 surface and boreholes rock samples covering the strata and magmatic rocks were tested and analyzed. A geothermal resource genesis model was built by combining field investigations, hydrochemical isotope, and rock thermal property analysis. The following conclusions have been made.

(1) The analytical results of the hydrochemical isotope indicate that the geothermal water in the Wugongshan area originated from precipitation and is recycled as water vapor.
(2) The results of the thermophysical tests indicate that the average radiogenic heat generation rate of lithologic rocks in different ages is 0.24–5.49 μW/m^3. The average thermal conductivity of rocks in the area ranges from 2.504 to 4.390 W/mK, the average specific heat of rocks in the study area ranges from 1.318 to 4.829 MJ/m^{3}K, and the average thermal diffusivity ranges from 1.115 to 1.611 × 10^{-6} m^2/s.
(3) The radiogenic heat generation rate is Jurassic granite, Silurian granite, Cambrian metamorphic rocks, siliceous quartzite, and quartz veins in order from the highest to the lowest. The average radioactive heat generation rate of Jurassic granite is 5.49 μW/m^3, which is higher than the global average of the radioactive heat generation rate of granite, indicating that the radioactive elements of Jurassic granite have a certain contribution to the heat flow.
(4) The genesis mechanism of geothermal water in the Wugongshan area is "heat generation of deep crust + thermal conduction of siliceous quartzite + heat transfer of shallow granite + heat accumulation of structures."

Data availability statement

The original contributions presented in the study are included in the article/Supplementary Material; further inquiries can be directed to the corresponding authors.

Author contributions

Conceptualization, KL and YZ; methodology, QH and KL; software, WJ; validation, SZ and XH; formal analysis, HZ and LW; investigation, YZ, SW, and XH; resources, KL and SW; data curation, LW and SW; writing—original draft preparation, KL and YZ; writing—review and editing, QH and KL; visualization, KL; supervision, KL; project administration, KL and XH; funding acquisition, KL. All authors have read and agreed to the published version of the manuscript.

Funding

This study was supported by the project of the China Geological Survey (DD20221677-2) and the Fundamental Research Funds of CGS Research (JKY202004).

Acknowledgments

The authors are grateful for the assistance during fieldwork provided by Jue Tong from The Fourth Geological Brigade of Jiangxi Geological Bureau, Jiangxi, China. The authors also thank Dr. Tingxi Yu of the China University of Geosciences (Beijing) and Junhan Guo of the Chinese Academy of Geological Sciences for the computer mapping work. The authors also would like to thank the professional reviewers and editors.

Conflict of interest

The authors declare that the research was conducted in the absence of any commercial or financial relationships that could be construed as a potential conflict of interest.

Publisher's note

All claims expressed in this article are solely those of the authors and do not necessarily represent those of their affiliated organizations, or those of the publisher, the editors, and the reviewers. Any product that may be evaluated in this article, or claim that may be made by its manufacturer, is not guaranteed or endorsed by the publisher.

References

Artemieva, I. M., Thybo, H., Jakobsen, K., Sørensen, N. K., and Nielsen, L. S. (2017). Heat production in granitic rocks: Global analysis based on a new data compilation granite 2017. *Earth-Sci. Rev.* 172, 1–26. doi:10.1016/j.earscirev.2017.07.003

Bai, B., Jiang, S., Liu, L., Li, X., and Wu, H. (2021a). The transport of silica powders and lead ions under unsteady flow and variable injection concentrations. *Powder Technol.* 387, 22–30. doi:10.1016/j.powtec.2021.04.014

Bai, B., Nie, Q., Zhang, Y., Wang, X., and Hu, W. (2021b). Cotransport of heavy metals and SiO_2 particles at different temperatures by seepage. *J. Hydrology* 597, 125771. doi:10.1016/j.jhydrol.2020.125771

Bai, D. H., Liao, Z. J., and Zhao, G. Z. (1994). Inference of magmatic heat source in Tengchong Rehai geothermal field from MT detection results. *Chin. Sci. Bull.* 4, 344–347.

Charvet, J. (2013). The neoproterozoic-early paleozoic tectonic evolution of the south China block: An overview. *J. Asian. Earth. Sci.* 74, 198–209. doi:10.1016/j.jseaes.2013.02.015

Chen, X., Zhang, Y. D., Fan, J. X., Cheng, J., and Li, Q. (2010). Ordovician graptolite-bearing strata in southern Jiangxi with a special reference to the Kwangsian Orogeny. *Sci. China (Earth Sci.* 53 (1), 1602–1610. doi:10.1007/s11430-010-4117-6

Cho, W., and Kwon, S. (2010). Estimation of the thermal properties for partially saturated granite. *Eng. Geol.* 115 (1-2), 132–138. doi:10.1016/j.enggeo.2010.06.007

Clauser, C. (2011). Thermal storage and transport properties of rocks, II: Thermal conductivity and diffusivity. *Encycl. Solid Earth Geophys.* 2, 1431–1448. doi:10.1007/978-90-481-8702-7_67

Côté, J., and Konard, J. M. (2005). Thermal conductivity of base-course materials. *Can. Geotech. J.* 42, 61–78. doi:10.1139/t04-081

Dor, J., and Zhao, P. (2000). *Characteristics and genesis of the yangbajing geothermal field, tibe*. Kyushu - Tohoku, Japan: Proceedings World Geothermal Congress. (English Edition).

Faure, M., Shu, L. S., Wang, B., Charvet, J., Choulet, F., and Monie, P. (2009). Intracontinental subduction: A possible mechanism for the early palaeozoic orogen of SE China. *Terra nova.* 21, 360–368. doi:10.1111/j.1365-3121.2009.00888.x

Faure, M., Sun, Y., Shu, L. S., Monié, P., and Charvet, J. (1996). Extensional tectonics within a subduction-type orogen. The case study of the Wugongshan dome (Jiangxi Province, southeastern China). *Tectonophysics* 263, 77–106. doi:10.1016/s0040-1951(97)81487-4

Feng, Y. F., Zhang, X. X., and Zhang, B., (2018) The geothermal formation mechanism in the Gonghe Basin: Discussion and analysis from the geological background[J]. *China Geol.*, 1(3):15.

Gao, S. Q., Liu, K., and Sun, W. J. (2020). Water chemistry and strontium isotope geochemistry characteristic of granitic banded thermal reservoirs. *Y. R.* 53 (08), 36–42+49.

Gustafsson, S. E. (1991). Transient plane source techniques for thermal conductivity and thermal diffusivity measurements of solid materials. *Rev. Sci. Instrum.* 62 (3), 797–804. doi:10.1063/1.1142087

Gustavsson, J. S., Gustavsson, M. K., and Gustafsson, S. E. (1997). On the use of the hot disk thermal constants analyser for measuring the thermal conductivity of thin samples of electrically insulating materials. *Therm. Conduct.* 24.

Gustavsson, M., Karawacki, E., and Gustafsson, S. E. (1994). Thermal conductivity, thermal diffusivity, and specific heat of thin samples from transient measurements with hot disk sensors. *Rev. Rev. Sci. Instrum.* 65 (12), 3856–3859. doi:10.1063/1.1145178

Gustavsson, M. K., and Gustafsson, S. E. (2005). On the use of transient plane source sensors for studying materials with direction dependent properties. *Therm. Conduct.* 26, 367–377.

He, Z. Y., Xu, X. S., and Niu, Y. L. (2010). Petrogenesis and tectonic significance of a Mesozoic granite–syenite–gabbro association from inland South China. *Lithos* 119, 621–641. doi:10.1016/j.lithos.2010.08.016

Hu, Z. H., Gao, H. L., and Wan, H. P. (2022). Temporal and spatial evolution of hydrothermal alteration in the yangbajing geothermal filed, xizang (Tibet). *Geol. Rev.* 68 (01), 359–374.

Jiang, G. Z., Gao, P., and Rao, S. (2016). Compilation of heat flow data in the continental area of China (4th edition). *Chin. J. Geophys* 59 (8), 2892–2910.

Jiang, M., Tan, H. d., and Zhang, Y. w. (2012). Geophysical mode of Mazhan-Gudong magma chamber in Tengchong volcano-tectonic area. *Acta Geosci. Sin.* 33 (05), 731–739.

John, L., Stefan, A., and Hjalti, F. (2005). *Geology, hy-drothermal alteration and fluid inclusion studies of olkaria domes geothermal field, Kenya*. English Edition. Antalya, Turkey: Proceedings World Geo-thermal Congress.

Jorand, R., Clauser, C., Marquart, G., and Pechnig, R. (2015). Statistically reliable petrophysical properties of potential reservoir rocks for geothermal energy use and their relation to lithostratigraphy and rock composition: The NE Rhenish Massif and the Lower Rhine Embayment (Germany). *Geothermics* 53, 413–428. doi:10.1016/j.geothermics.2014.08.008

Li, J. H., Cawood, P. A., Ratschbacher, L., Zhang, Y., Dong, S., Xin, Y., et al. (2019). Building southeast China in the late mesozoic: Insights from alternating episodes of shortening and extension along the lianhuashan fault zone. *Earth-Sci. Rev.* 201, 103056. doi:10.1016/j.earscirev.2019.103056

Li, W. X., Li, X. H., Li, Z. X., and Lou, F. S. (2008). Obduction-type granites within the NE Jiangxi ophiolite: Implications for the final amalgamation between the Yangtze and Cathaysia blocks. *Gondwana Res.* 13, 288–301. doi:10.1016/j.gr.2007.12.010

Li, X. C., Ma, Z. Y., and Z, X. L. (2016). Genetic model of the dongda geothermal field in Guanzhong basin, Shaanxi province. *Geol. China* 43 (6), 2082–2091.

Li, X. H., Li, W. X., Li, Z. X., Lo, C. H., Jian, W., Ye, M. F., et al. (2009). Amalgamation between the Yangtze and Cathaysia blocks in South China: Constraints from SHRIMP U-Pb zircon ages, geochemistry and Nd-Hf isotopes of the shuangxiwu volcanic rocks. *Precambrian Res.* 174 (1-2), 117–128. doi:10.1016/j.precamres.2009.07.004

Li, Z. X. (1998). Tectonic history of the major East Asian lithospheric blocks since the mid-Proterozoic-A synthesis. *A G. U, Geodyn. Ser.* 27, 221–243.

Lin, W. J., Chen, X. Y., and Liu, G, H. N. (2020). Geothermal, geological characteristics and exploration direction of hot dry rocks in the Xiamen bay-Zhangzhou basin, southeastern China. *Acta Geo Sin.* 94 (07), 2066–2077.

Liu, F., Wang, G. L., and Zhang, W. (2020). Terrestrial heat flow and geothermal Genesis mechanism of geothermal resources in northern Ningdu County, Jiangxi Province. *Chin. Geo Bull.* 39 (12), 1883–1890.

Liu, K., Wang, S. S., and Sun, Y. (2017). Characteristics and regionalization of geothermal resources in Beijing. *Geol. China* 44 (6), 1128–1139.

Liu, S. W., Wang, L. S., and Li, C. (2006). Lithospheric thermo-rheological structure and cenozoic thermal regime in the tarim basin, northwest China. *Acta Geol. Sin.* 80 (3), 344–350.

Long, D. H., Zhou, X. L., and Yang, K. G. (2021). Research on relationship between the deep structure and geothermal resource distribution in the northeastern Tibetan Plateau. *Geol. China* 48 (03), 721–731.

Lou, F. S., Shen, W. Z., and Wang, D. Z. (2005). Ziron U-Pb isotopic chronology of the Wugongshan dome compound granite in Jiangxi province. *Acta Geol. Sin.* 79 (05), 636–644.

Lou, F. S., Shu, L. S., and Yu, J. H. (2002). Petrological and geochemical characteristics and origin of the Wugongshan dome granite, Jiangxi province. *Geol. Rev.* 48 (01), 80–88.

Lu, S., Ren, T., Gong, Y., and Horton, R. (2007). An improved model for predicting soil thermal conductivity from water content at room temperature. *Soil Sci. Soc. Am. J.* 71, 8–14. doi:10.2136/sssaj2006.0041

Luo, Lu., Zhu, X., He, C. y., and Mao, X. (2019). Study on the Genesis of geothermal fluid in Xianyang geothermal filed. *Geol. Rev.* 65 (06), 1422–1430.

Miao, S. Q., and Zhou, Y. S. (2017). Measuring thermal diffusivity and conductivity of sandstone at high temperatures using a laser flash method. *Bull. Mineral. Petrol. Geochem.* 36 (3), 450–454.

Mihiretie, B. M., Cederkrantz, D., Rosen, A., Otterberg, H., Sundin, M., Gustafsson, S., et al. (2017). Finite element modeling of the hot disc method. *Int. J. Heat. Mass Transf.* 115 (B), 216–223. doi:10.1016/j.ijheatmasstransfer.2017.08.036

Mihiretie, B. M., Cederkrantz, D., Sundin, M. A., Rosén, A., Otterberg, H., Hinton, Å., et al. (2016). Thermal depth profiling of materials for defect detection using hot disk technique. *Aip Adv.* 6 (8), 085217. doi:10.1063/1.4961879

Qin, D. J., Turner, J. V., and Pang, Z. H. (2005). Hydrogeochemistry and groundwater circulation in the Xi'an geothermal field, China. *Geothermics* 34, 471–494. (English Edition). doi:10.1016/j.geothermics.2005.06.004

Qu, Z. W., Zhang, H., and Hu, Y. Z. (2019). General situation and development regional division of geothermal resources in Western Sichuan region. *Geotech. Eng. World* 10 (05), 1233–1242.

Ren, J. S. (1991). On the geotectonics of southern China. *Acta Geol. Sin.* 4 (2), 111–130.

Rybach, L. (1976). Radioactive heat production in rocks and its relation to other petrophysical parameters. *Pure Appl. Geophys.* 114 (2), 309–317. doi:10.1007/bf00878955

Shao, J. A., and Zhang, W. L. (2008). The evolving rift belt-Wudalianchi volcanic rock belt. *Earth Sci. Front.* 15 (06), 241–250.

Shu, L. S., Sun, Y., and Wang, D. Z. (1998). Mesozoic extensional structure of wugongshan, south China. *Sci. China (Series D.* 28 (5), 431–438.

Shu, L. S., Wang, D. Z., and Shen, W. Z. (2000). Nd-Sr isotopic compositions of granitic rocks of the Mesozoic metamorphic core complex in the Wugongshan area, Jiangxi province. *J. Nanjing Univ. Nat. Sci.* 36 (03), 306–311.

Sizov, A., Cederkrantz, D., Salmi, L., Rosén, A., Jacobson, L., Gustafsson, S. E., et al. (2016). Thermal conductivity versus depth profiling of inhomogeneous materials using the hot disc technique. *Rev. Sci. Instrum.* 87 (7), 797–377. doi:10.1063/1.4954972

Sun, Y., Shu, L. S., and Faure, M. (1994). Extensional structure of the granite dome of the Wugongshan mountain in the northern Jiangxi province. *J. Nanjing Univ. Nat. Sci.* 04, 633–637.

Sun, Y., Shu, L. S., and Faure, M. (1997). Tectonic development of the metamorphic core complex of the Wugongshan in the northern Jiangxi province. *J. Nanjing Univ. Nat. Sci.* 33 (3), 447–449.

Sven, F. (2018). The variability of rock thermal properties in sedimentary basins and the impact on temperature modelling – A Danish example. *Geothermics* 76, 1–14. doi:10.1016/j.geothermics.2018.06.006

Tang, X. C., Wang, G. L., and Ma, Y. (2020). Geological model of heat source and accumulation for geothermal anomalies in the Gonghe basin, northeastern Tibetan Plateau. *Acta Geol. Sin.* 94 (07), 2052–2065.

Vilà, M., Fernández, M., and Jiménez-Munt, I. (2010). Radiogenic heat production variability of some common lithological groups and its significance to lithospheric thermal modeling. *Tectonophysics* 490 (3–4), 152–164. doi:10.1016/j.tecto.2010.05.003

Wan, J. J., Sun, Z. X., and Hu, B. Q. (2013). Radiogenic geochemistry investigation on granitic rocks from Fogang complex, Northern Guangdong province and its implications for Hot Dry Rock resource. *Geol. Bull.* 39 (12), 1883–1890.

Wang, G. L., Wang, W. L., Zhang, W., Ma, F., and Liu, F. (2020). The status quo and prospect of geothermal resources exploration and development in Beijing-Tianjin-Hebei region in China. *China Geol.* 3 (1), 173–181. doi:10.31035/cg2020013

Wang, G. L., and Lin, W. J. (2020). Main hydro-geothermal systems and their genetic models in China. *Acta Geol. Sin.* 94 (07), 1923–1937.

Wang, J. Y., Zhang, J., and Xu, H. H. (2015). *Geothermics and its applications*. Beijing: Science Press.

Wu, S. S., Dai, K. M., and Wang, J. C. (2021). Analysis of fault structure and geothermal resources in Yangshan area, Nanjing City. *J. Hefei Univ. Technol. Nat. Sci.* 44 (06), 834–839.

Xia, J. W. (1995). Cause of Yanchihe hot spring in the west Hubei and its influence on crustal stability of the Shuibuya water control project. *Crustal Deformation Earthq.* 47, 70–76.

Xia, Z. z., Ma, Z. x., and Wang, X. g. (2017). Progress of the geothermal exploration projects sponsored by Jiangxi administration fund for geological exploration. *J. China Text. Univ. Engl. Ed.* . 40 (01), 71–78.

Xin, S. L., Wang, J. L., and Dou, H. P. (2014). Experiments and analyses of thermal physical property of rocks and its effect factor on buried hill resource. *Mineral. Petrol.* 34 (4), 102–107.

Xue, J. Q., Gan, B., and Li, B. X. (2013). Geological-Geophysical characteristics of enhanced geothermal systems (HOT DRY ROCKS) in Gonghe-Guide basin. *Geophys. Geochem. Explor.* 37 (01), 35–41.

Zhang, B. J., Zhao, T., Li, Y. Y., Xing, Y. F., Zhang, D. L., Gao, J., et al. (2019). The hydrochemical characteristics and its significance of geothermal water in both sides of large fault: Taking northern section of the liaokao fault in north China as an example. *China Geol.* 2 (4), 512–521. doi:10.31035/cg2018132

Zhang, C., Jiang, G. Z., Shi, Y., Wang, Z., Wang, Y., Li, S., et al. (2018a). Terrestrial heat flow and crustal thermal structure of the Gonghe-Guide area, northeastern Qinghai-Tibetan plateau. *Geothermics* 72, 182–192. (English Edition). doi:10.1016/j.geothermics.2017.11.011

Zhang, C., Wei, X. D., and Yang, H. T. (2018b). Characteristics of Olkaria geothermal field, a rift volcanic geothermal system. *Sino-Global Energy.* 23 (12), 16–21.

Zhang, L. H., Guo, Z. F., and Zheng, G. D. (2017). Flux and Genesis of greenhouse gases emissions from cenozoic volcanic-geothermal fields, South Tibet: A case study of volcanic-geothermal fields in gulu-yadong rift. *Acta Petrol. Sin.* 33 (01), 250–266.

Zhang, Y. Y., Liu, Kai., and He, Q. C. (2022). Zircon U-Pb ages, Hf isotopic characteristics, and geological significance of the Mesozoic granites in Wugong Mountains area. *Jiangxi. Geol. Rev.* 68 (04), 1301–1319.

Zhao, C. P., Ran, H., and Wang, Y. (2012). Present-day mantle-derived helium release in the Tengchong volcanic field,Southwest China: Implications for tectonics and magmatism. *Acta Petrol. Sin.* 28 (4), 1189–1204.

Zhao, G. C., and Guo, J. H. (2012). Precambrian geology of China: Preface. *Precambrian Res.* 222-223, 1–12. doi:10.1016/j.precamres.2012.09.018

Zhao, P., Mack, K., and Dor, J. (2001). Noble gases constraints on the origin and evolution of geothermal fluids from the Yangbajing geothermal field, Tibet. *Acta Petrol. Sin.* 17 (3), 497–503.

Zhao, P., Wang, J. Y., and Wang, J. A. (1995). Characteristics of heat production distribution in SE China. *Acta Petrol. Sin.* 36 (3), 450–454.

Zhou, Y., Mu, G. X., Zhang, H., Zhang, P., Shi, H., Chen, S., et al. (2017). An abnormal bone marrow microenvironment contributes to hematopoietic dysfunction in Fanconi anemia. *Geol. China* 44 (5), 1017–1027. doi:10.3324/haematol.2016.158717